

On the near-threshold peak structure in the differential cross section of ϕ -meson photoproduction: missing resonance with non-negligible strangeness content?

Alvin Kiswandhi and Shin Nan Yang

Center for Theoretical Sciences, National Taiwan University, Taipei 10617, Taiwan

Department of Physics, National Taiwan University, Taipei 10617, Taiwan

(Dated: June 3, 2019)

The details of the analysis, with more extensive results, of the near-threshold bump structure in the forward differential cross section of the ϕ -meson photoproduction to determine whether it is a signature of a resonance are presented. The analysis is carried out in an effective Lagrangian approach which includes Pomeron and (π, η) exchanges in the t channel, and contributions from the s - and u -channel excitation of a postulated nucleon resonance. In addition to the differential cross sections, we use the nine spin-density matrix elements as recently measured, instead of the ϕ -meson decay angular distributions which depend only on six spin-density matrix elements as was done before, to constrain the resonance parameters. We conclude that indeed the bump structure as reported by LEPS, can only be explained with an assumption of the excitation of a resonance of spin $3/2$, as previously reported. However, both parities of (\pm) can account for the data equally well with almost identical mass of 2.08 ± 0.04 GeV and width of 0.501 ± 0.117 and 0.570 ± 0.159 for $3/2^-$ and $3/2^+$, respectively. The ratio of the helicity amplitudes $A_{1/2}/A_{3/2}$ calculated from the resulting coupling constants differs in sign from that of the known $D_{13}(2080)$. More experimental data on single and double polarization observables are needed to resolve the parity. We further find that with an assumption of large values of the OZI-evading parameters $x_{\text{OZI}} = 12$ for $J^P = 3/2^-$ and $x_{\text{OZI}} = 9$ for $J^P = 3/2^+$, the discrepancy between the recent experimental data on ω -meson photoproduction and theoretical model can be considerably reduced. We argue that the large value of x_{OZI} indicates that the postulated resonance contains non-negligible amount of strangeness content.

PACS numbers: 13.60.Le, 25.20.Lj, 14.20.Gk

I. INTRODUCTION

The ϕ -meson photoproduction reaction has long been extensively studied. At high energy, diffractive process dominates and it can be well described by t -channel Pomeron (P) exchange [1, 2]. In the low-energy region, the nondiffractive processes of the pseudoscalar (π, η) -meson exchange are also known to contribute [1]. Other processes, such as nucleon exchange [3, 4], nucleon resonances [5, 6], second Pomeron exchange, t -channel scalar meson and glueball exchanges [6, 7], and $s\bar{s}$ -cluster knockout [4, 8, 9] have also been investigated. However, a peak in the differential cross sections of ϕ photoproduction on protons at forward angles around $E_\gamma \sim 2.0$ GeV as recently observed by the LEPS collaboration [10] cannot be explained by the processes mentioned above.

Since a bump in the cross sections is often associated with excitation of resonances, it is then tempting to see if the peak observed in [10] can be described by a resonance. There exist previous works studying the effects of resonances in s - and u -channels with masses up to 2 GeV [5, 6]. Ref. [5] employs $\text{SU}(6) \otimes \text{O}(3)$ symmetry within a constituent quark model and included explicitly excited resonances with quantum numbers $n \leq 2$. On the other hand, Ref. [6] includes all the known 12 resonances below 2 GeV listed in Particle Data Group [11], with coupling constants determined by available experimental data [12, 13] at large momentum transfers. The resonances are found to play significant roles in the polarization observables. Nevertheless, the resonances con-

sidered, either listed in PDG table or predicted by some quark model, cannot describe the nonmonotonic behavior as reported in [10].

In [14], we have tried to explore the possibility on whether such a nonmonotonic behavior could be explained by a postulated resonance by fiat in the neighborhood of observed peak position. We found that, with an addition of a resonance of spin- $3/2$ to a background mechanism which consists of Pomeron and (π, η) -meson exchange in t -channel, not only the peak in the forward differential cross section but also the t -dependence of differential cross section (DCS) and ϕ meson decay angular distribution can be well described. Similar attempt was also made in [15], where the effect of the $K\Lambda(1520)$ is taken into account in a coupled-channel analysis. Their results preferred a resonance of $J^P = 1/2^-$. However, the calculation is marred by a mistake in the phase of the Pomeron amplitude.

In this paper, we give the details of our previous analysis [14] and present extensive results of our calculation. In addition, we now use the new LEPS data [16] which consisted of nine spin-density matrix elements measured at three different energies to determine the resonance parameters, instead of the decay angular distributions of the ϕ meson, which involve only six spin-density matrix elements, taken only at two energies given in [10], as was done before. The use of a larger data set with better precision should provide a more stringent constraint on the model and gives rise to more reliable extracted resonance properties. We also provide an estimation of the strangeness content of the postulated resonance.

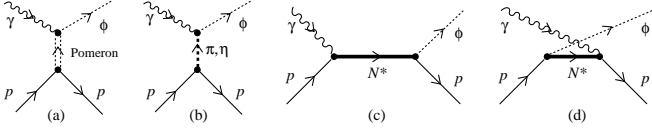


FIG. 1: Pomeron exchange, t -, s -, u -channel diagrams for $\gamma p \rightarrow \phi p$ reaction are labeled (a), (b), (c), and (d), respectively. Time runs from right to left.

This paper is organized as follows. The model used in our analysis, which consists of Pomeron and (π, η) -meson exchange in t -channel, and a postulated resonance is given in Sec. II. The extracted resonance parameters, their possible effects in the polarization observables and ω photoproduction, as well as an estimation of the strangeness content of the resonance, are presented in Sec. III. The summary is given in Sec. IV.

II. THE MODEL FOR ϕ MESON PHOTOPRODUCTION

We first introduce the kinematic variables k , p_i , q , and p_f for the four-momenta of the incoming photon, initial proton, outgoing ϕ -meson, and final proton, respectively, with $s = (k + p_i)^2 = (q + p_f)^2$, $t = (q - k)^2 = (p_f - p_i)^2$, and $u = (p_f - k)^2 = (q - p_i)^2$. We follow the convention of PDG [11] and define the invariant amplitude $-i\mathcal{M}$ is related to the S -matrix by

$$S_{fi} = \delta_{fi} - i \frac{(2\pi)^4 \delta^{(4)}(p_f + q - p_i - k)}{(2E_{\mathbf{p}_f})^{1/2} (2E_{\mathbf{p}_i})^{1/2} (2E_{\mathbf{q}})^{1/2} (2E_{\mathbf{k}})^{1/2}} \mathcal{M}_{fi}, \quad (1)$$

with normalization $\langle p_f | p_i \rangle = (2\pi)^3 \delta^{(3)}(\mathbf{p}_f - \mathbf{p}_i)$ for free-particle momentum state and $\bar{u}(p, s)u(p, s) = 2m$ for Dirac spinor with mass m . In addition to the background mechanism of Pomeron-exchange, t -channel π - and η -exchange, we will postulate the existence of a resonance by fiat and see whether we could describe the data of LEPS [10, 16]. We can then write the full amplitude \mathcal{M} as

$$\mathcal{M}_{fi} = \mathcal{M}_P + \mathcal{M}_{\pi+\eta} + \mathcal{M}_{N^*}, \quad (2)$$

as shown in Fig. 1, where \mathcal{M}_{N^*} contains both s - and u -channel contributions. The unpolarized differential cross section is related to the invariant amplitude by

$$\frac{d\sigma}{dt} = \frac{1}{64\pi s |\mathbf{k}_{cm}|^2} \frac{1}{4} \sum_{\lambda_N, \lambda_\gamma} \sum_{\lambda_{N'}, \lambda_\phi} |\mathcal{M}_{fi}|^2, \quad (3)$$

with \mathbf{k}_{cm} is the photon three momentum in the center-of-mass (CM) frame and λ_N , $\lambda_{N'}$, λ_γ and λ_ϕ denote the helicities of the initial proton, final proton, incoming photon, and outgoing ϕ -meson, respectively.

A. Pomeron exchange

Following Refs. [6, 17], we can easily write down the Pomeron-exchange amplitude of Fig. 1(d),

$$\mathcal{M}_P = -\bar{u}(p_f, \lambda_{N'}) M(s, t) \Gamma^{\mu\nu} u(p_i, \lambda_N) \times \varepsilon_\mu^*(q, \lambda_\phi) \varepsilon_\nu(k, \lambda_\gamma), \quad (4)$$

where $\varepsilon_\mu(q, \lambda_\phi)$ and $\varepsilon_\nu(k, \lambda_\gamma)$ are the polarization vectors of the ϕ -meson and photon with λ_ϕ and λ_γ , respectively, and $u(p_i, \lambda_N)[\bar{u}(p_f, \lambda_{N'})]$ is the Dirac spinor of the nucleon with momentum $p_i(p_f)$ and helicity $\lambda_N(\lambda_{N'})$. The transition operator $\Gamma^{\mu\nu}$ in Eq. (4) is

$$\Gamma^{\mu\nu} = \left(g^{\mu\nu} - \frac{q^\mu q^\nu}{q^2} \right) \not{k} - \left(k^\mu - \frac{k \cdot q q^\mu}{q^2} \right) \gamma^\nu - \left(\gamma^\mu - \frac{\not{q} q^\mu}{q^2} \right) \left[q^\nu - \frac{k \cdot q (p_i^\nu + p_f^\nu)}{k \cdot (p_i + p_f)} \right]. \quad (5)$$

The scalar function $M(s, t)$ is described by the Reggeon parametrization,

$$M(s, t) = C_P F_1(t) F_2(t) \frac{1}{s} \left(\frac{s - s_{th}}{s_0} \right)^{\alpha_P(t)} \times \exp \left[-\frac{i\pi}{2} \alpha_P(t) \right], \quad (6)$$

where the Pomeron trajectory is taken to be $\alpha_P(t) = 1.08 + 0.25t$ and $s_0 = (m_N + m_\phi)^2$. $F_1(t)$, the isoscalar form factor of the nucleon and $F_2(t)$, the form factor of the ϕ -photon-Pomeron coupling are given as [2, 6],

$$F_1(t) = \frac{4m_N^2 - a_N^2 t}{(4m_N^2 - t)(1 - t/t_0)^2}, \quad (7)$$

$$F_2(t) = \frac{2\mu_0^2}{(1 - t/m_\phi^2)(2\mu_0^2 + m_\phi^2 - t)}, \quad (8)$$

with $\mu_0^2 = 1.1 \text{ GeV}^2$, $a_N^2 = 2.8$, and $t_0 = 0.7 \text{ GeV}^2$.

In this study, we follow Ref. [6] by choosing the strength factor $C_P = 3.65$, which is obtained by fitting to the total cross sections data at high energy. In addition, we include a threshold factor s_{th} as was done in Refs. [3, 6] in order to get a better agreement with experimental data near the threshold region. If $s_{th} = 0$ is chosen as done in Ref. [6], a problem arises. Namely, the results for forward differential cross sections would overestimate the experimental data by about 20% as seen in Fig. 2 around $E_\gamma = 6 \text{ GeV}$. Since pomeron properties and behaviors at lower energies are not well-established, we adjust this parameter to fit the experimental data on the differential cross sections around $E_\gamma = 6 \text{ GeV}$. $E_\gamma = 6 \text{ GeV}$ is chosen because at this energy, one can reasonably expect that all other contributions from hadronic intermediate states would become negligible and only pomeron contributes. Furthermore, around this energy, experimental data are quite reliable in that they have relatively small error bars and rise

steadily without much fluctuation. These give us confidence to match the pomeron contribution to the experimental data at this energy by fixing $s_{th} = 1.3 \text{ GeV}^2$.

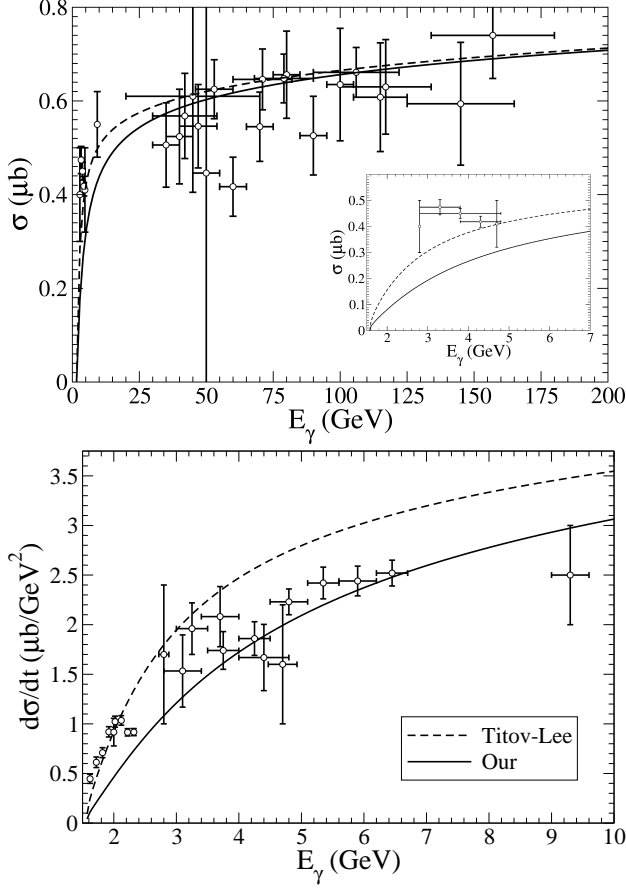


FIG. 2: Upper: total cross sections of ϕ photoproduction as a function of photon lab energy E_γ . Lower: differential cross sections of ϕ photoproduction at forward angle as a function of photon lab energy E_γ . Results of Ref. [6] (Titov-Lee) and this work (Our) are drawn as full and dashed lines, respectively. Data is taken from Ref. [19].

B. π and η -meson exchange

The amplitudes for the π - and η -exchange in t -channel, Fig. 1(c) in a straightforward manner [8, 9] and are given by

$$\begin{aligned} \mathcal{M}_{\pi+\eta} = & \frac{-eg_{\gamma\phi\pi}g_{\pi NN}F_\pi^2(t)}{m_\phi} \bar{u}(p_f, \lambda_{N'}) \gamma_5 \frac{\varepsilon^{\mu\nu\rho\sigma} q_\mu k_\rho}{t - m_\pi^2} \\ & \times u(p_i, \lambda_N) \varepsilon_\nu^*(q, \lambda_\phi) \varepsilon_\sigma(k, \lambda_\gamma) + \\ & - \frac{eg_{\gamma\phi\eta}g_{\eta NN}F_\eta^2(t)}{m_\phi} \bar{u}(p_f, \lambda_{N'}) \gamma_5 \frac{\varepsilon^{\mu\nu\rho\sigma} q_\mu k_\rho}{t - m_\eta^2} \\ & \times u(p_i, \lambda_N) \varepsilon_\nu^*(q, \lambda_\phi) \varepsilon_\sigma(k, \lambda_\gamma), \end{aligned} \quad (9)$$

with the coupling constants $g_{\pi NN}$, $g_{\gamma\phi\pi}$, and $g_{\gamma\phi\eta}$, as well as the form factors $F_\pi(t)$ and $F_\eta(t)$ for the virtually exchanged mesons at the MNN and $\gamma\phi M$ ($M = \pi, \eta$) vertices, respectively, are taken to be the same as in Ref. [17]. We choose $g_{\eta NN} = 1.12$ [20] and $\Lambda_\pi = \Lambda_\eta = 1.2 \text{ GeV}$ which are slightly different with the values given in Ref. [17] ($g_{\eta NN} = 1.94$, and $\Lambda_\pi = \Lambda_\eta = 1.05 \text{ GeV}$). As we see in Fig. 3, the choice of cut-off parameters Λ_π and Λ_η appears to be in a better agreement with Ref. [18] than the choice of $\Lambda_\pi = 0.6 \text{ GeV}$ used in Ref. [6] in the low- t region, which is the region of interest in this present work.

C. Excitation of Baryon Resonance

The Feynman diagrams with an N^* in the intermediate state in s - and u -channel are shown in Fig. 1(a) and (b). To evaluate the invariant amplitudes involving N^* , we use the following interaction Lagrangians. For the coupling of spin-1/2 and 3/2 resonances to γN , we choose the commonly used interaction Lagrangians [20–22]

$$\mathcal{L}_{\gamma NN^*}^{1/2^\pm} = eg_{\gamma NN^*}^{(2)} \bar{\psi}_N \Gamma^\pm \sigma_{\mu\nu} F^{\mu\nu} \psi_{N^*} + \text{h.c.}, \quad (10)$$

$$\begin{aligned} \mathcal{L}_{\gamma NN^*}^{3/2^\pm} = & ieg_{\gamma NN^*}^{(1)} \bar{\psi}_N \Gamma^\pm (\partial^\mu \psi_{N^*}^\nu) \tilde{F}_{\mu\nu} \\ & + eg_{\gamma NN^*}^{(2)} \bar{\psi}_N \Gamma^\pm \gamma^5 (\partial^\mu \psi_{N^*}^\nu) F_{\mu\nu} + \text{h.c.}, \end{aligned} \quad (11)$$

where $F_{\mu\nu} = \partial_\mu A_\nu - \partial_\nu A_\mu$ is the electromagnetic field tensor, and $\sigma_{\mu\nu} = \frac{i}{2}(\gamma_\mu \gamma_\nu - \gamma_\nu \gamma_\mu)$. Also, $\tilde{F}_{\mu\nu} = \frac{1}{2}\epsilon_{\mu\nu\alpha\beta} F^{\alpha\beta}$ denotes the dual electromagnetic field tensor with $\epsilon^{0123} = +1$. The operator Γ^\pm are given by $\Gamma^+ = 1$ and $\Gamma^- = \gamma_5$. For the ϕNN^* interaction Lagrangians,

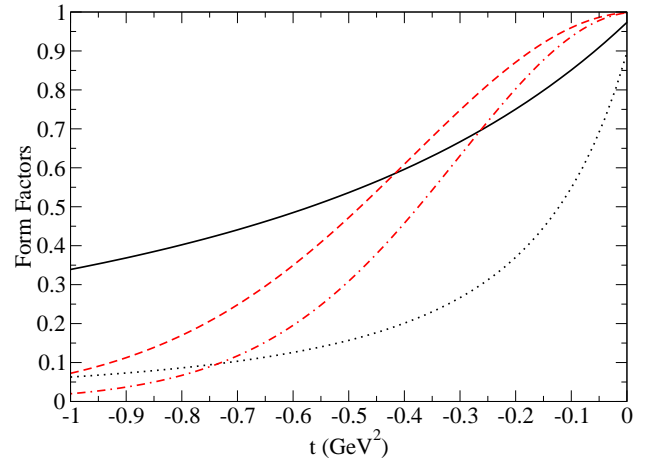


FIG. 3: Comparison between form factors with different cut-off parameters for the t -channel diagram involving intermediate π . Full and dotted black lines show the form factors used here with cut-off parameters $\Lambda = 1.2 \text{ GeV}$ and $\Lambda = 0.6 \text{ GeV}$, respectively, while dashed and dash-dotted red lines show the form factors denoted by “K10” and “T10” in Ref. [18], respectively.

we have

$$\begin{aligned}\mathcal{L}_{\phi NN^*}^{1/2^\pm} &= g_{\phi NN^*}^{(1)} \bar{\psi}_N \Gamma^\pm \gamma^\mu \psi_{N^*} \phi_\mu \\ &+ g_{\phi NN^*}^{(2)} \bar{\psi}_N \Gamma^\pm \sigma_{\mu\nu} G^{\mu\nu} \psi_{N^*} + \text{h.c.},\end{aligned}\quad (12)$$

$$\begin{aligned}\mathcal{L}_{\phi NN^*}^{3/2^\pm} &= ig_{\phi NN^*}^{(1)} \bar{\psi}_N \Gamma^\pm (\partial^\mu \psi_{N^*}^\nu) \tilde{G}_{\mu\nu} \\ &+ g_{\phi NN^*}^{(2)} \bar{\psi}_N \Gamma^\pm \gamma^5 (\partial^\mu \psi_{N^*}^\nu) G_{\mu\nu} \\ &+ ig_{\phi NN^*}^{(3)} \bar{\psi}_N \Gamma^\pm \gamma^5 \gamma_\alpha (\partial^\alpha \psi_{N^*}^\nu - \partial^\nu \psi_{N^*}^\alpha) (\partial^\mu G_{\mu\nu}) \\ &+ \text{h.c.},\end{aligned}\quad (13)$$

where $G^{\mu\nu}$ is defined as $G^{\mu\nu} = \partial^\mu \phi^\nu - \partial^\nu \phi^\mu$ with ϕ^μ the field of ϕ -meson. The dual field tensor $\tilde{G}_{\mu\nu}$ is again defined in the same way as its electromagnetic counterpart with $F^{\alpha\beta} \rightarrow G^{\alpha\beta}$. Notice that we could have chosen to describe the γNN^* in the same way as we describe the ϕNN^* interactions. However, current conservation consideration fixes $g_{\gamma NN^*}^{(1)}$ for $J^P = 1/2^\pm$ resonances to be zero. In addition, the term proportional to $g_{\gamma NN^*}^{(3)}$ in the Lagrangian densities of Eq. (13) vanishes in the case of real photon. Then, the full invariant amplitude of s - and u -channels can be obtained straightforwardly by following the Feynman rules.

The form factor for the vertices used in the s - and u -channel diagrams, $F_{N^*}(p^2)$, is taken to be similar as in Ref. [18]

$$F_{N^*}(p^2) = \frac{\Lambda^4}{\Lambda^4 + (p^2 - M_{N^*}^2)^2}, \quad (14)$$

with Λ is the cut-off parameter for the virtual N^* . In this work, we choose $\Lambda = 1.2$ GeV for all resonances. The spin-1/2 N^* propagator can be written in a Breit-Wigner form as

$$G^{(1/2)}(p) = \frac{i(\not{p} + M_{N^*})}{p^2 - M_{N^*}^2 + iM_{N^*}\Gamma_{N^*}}, \quad (15)$$

with Γ_{N^*} the total decay width of N^* . The Rarita-Schwinger propagator is used for the spin-3/2 N^*

$$\begin{aligned}G_{\mu\nu}^{(3/2)}(p) &= \frac{i(\not{p} + M_{N^*})}{p^2 - M_{N^*}^2 + iM_{N^*}\Gamma_{N^*}} \left[-g_{\mu\nu} + \frac{1}{3}\gamma_\mu\gamma_\nu \right. \\ &\quad \left. - \frac{1}{3M_{N^*}}(p_\mu\gamma_\nu - p_\nu\gamma_\mu) + \frac{2}{3M_{N^*}^2}p_\mu p_\nu \right].\end{aligned}\quad (16)$$

Because $u < 0$, we take $\Gamma_{N^*} = 0$ MeV for the propagator in the u channel.

It should, however, be stressed that, we do not know the value of the coupling constants $g_{\phi NN^*}$ and $g_{\gamma NN^*}$, as our calculations are done in the tree level. Therefore, in present calculation, we show the values of $g_{\gamma NN^*}g_{\phi NN^*}$ obtained by fitting the experimental data. The parameters for the resonances tried are given in Tab. I.

III. RESULTS AND DISCUSSIONS

In this section, we first present our model predictions for the differential cross sections, spin-density matrix elements, and decay angular distributions and compare them with the data for both the cases with $3/2^-$ and $3/2^+$ resonances. We

A. Differential cross sections, spin-density matrix elements, and decay angular distributions

With the model presented in Sec. II, one can easily obtain the full amplitude of $\gamma p \rightarrow \phi p$ reaction and calculate the scattering observables straightforwardly with a specific assignment of spin-parity of the resonance. Since the peak appears to lie close to the ϕN threshold, only the lower partial waves are important and we shall consider only $J^P = 1/2^\pm, 3/2^\pm$ as the possible candidates for the spin-parity assignment of the resonance. In this

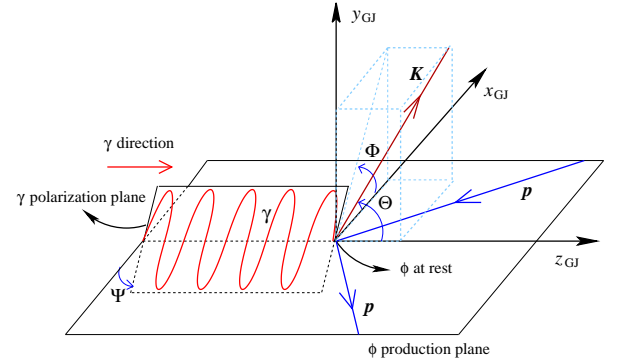


FIG. 4: The ϕ photoproduction in Gottfried-Jackson system.

work, we fit our model simultaneously to differential cross section at forward angle as a function of photon energy and differential cross sections dependence on t at eight photon energies reported in [10], as well as to nine spin-density matrix elements ρ_{ij}^α [24] as a function of t at three photon energies [16]. We use the Gottfried-Jackson system, in which ϕ -meson is at rest, as depicted in Fig. 4, to analyze the spin-density matrix elements. The z_{GJ} axis is taken to be along the incoming photon momentum while y_{GJ} axis is taken to be along $\mathbf{p}_f \times \mathbf{p}_i$ direction, with \mathbf{p}_f and \mathbf{p}_i the three-momentum of final and initial proton, respectively. The x_{GJ} axis is chosen to form a right-handed coordinate system.

Notice that in our previous work [14], decay angular distributions W , instead of the spin-density matrix elements ρ_{ij}^α were used in the data set to which we fit our model parameters. Even though the decay angular distributions are also functions of spin-density matrix elements (SDME), they depend only on only six out of a total of nine SDMEs. Furthermore, the decay angular distributions used in [14], as presented in [10], are taken only at

TABLE I: The N^* parameters for $J^P = 3/2^\pm$ resonances together with their errors obtained by HESSE method of MINUIT package.

	$J^P = 3/2^+$	$J^P = 3/2^-$
$M_{N^*}(\text{GeV})$	2.08 ± 0.04	2.08 ± 0.04
$\Gamma_{N^*}(\text{GeV})$	0.501 ± 0.117	0.570 ± 0.159
$eg_{\gamma NN^*}^{(1)} g_{\phi NN^*}^{(1)}$	0.003 ± 0.009	-0.205 ± 0.083
$eg_{\gamma NN^*}^{(1)} g_{\phi NN^*}^{(2)}$	-0.084 ± 0.057	-0.025 ± 0.017
$eg_{\gamma NN^*}^{(1)} g_{\phi NN^*}^{(3)}$	0.025 ± 0.076	-0.033 ± 0.017
$eg_{\gamma NN^*}^{(2)} g_{\phi NN^*}^{(1)}$	0.002 ± 0.006	-0.266 ± 0.127
$eg_{\gamma NN^*}^{(2)} g_{\phi NN^*}^{(2)}$	-0.048 ± 0.047	-0.033 ± 0.032
$eg_{\gamma NN^*}^{(2)} g_{\phi NN^*}^{(3)}$	0.014 ± 0.040	-0.043 ± 0.032
χ^2/N	0.891	0.821

two photon energies and averaged over t , while the nine SDMEs used in this work as presented in [16] are taken at three photon energies and are functions of t . We expect that the larger set of data considered in this work would provide a more stringent constraint on our model and results.

In tree-level approximation, only products like $g_{\gamma NN^*} g_{\phi NN^*}$ enter. The other parameters in our model are the resonance mass and width. They are determined with the use of MINUIT by fitting to the data measured at SPring8 [10, 16] as described in the previous paragraphs.

It is found that with assignment of spin-parity $J^P = 1/2^\pm$ for the resonance, it is not possible to explain the nonmonotonic behavior in the forward differential cross section near threshold reported in [10]. It is worthwhile to note that in the constituent quark model of Refs. [25, 26], spin-1/2 resonances are also not predicted to be of significant contribution at around $E_\gamma = 2$ GeV. Our results seem to be in line with their prediction.

On the other hand, we find that the experimental data can be well described with a spin-parity assignment of either $J^P = 3/2^-$ or $J^P = 3/2^+$ for the postulated resonance, both with comparable (mass, width) of (2.08, 0.570) and (2.08, 0.501) GeV, respectively. The quality of the agreement between data and model predictions for both spin-parity assignments is similar even though the resulting χ^2 value is slightly smaller for the case $J^P = 3/2^-$ as seen in Table I where the values of the products of $g_{\gamma NN^*} g_{\phi NN^*}$ are also presented. We note that even though the obtained values for the mass and width for both $3/2^\pm$ are almost identical, the products of the coupling constants are quite different.

The results of our best fit, as compared to the data of [10, 16], are shown in Figs. 5–9 where the dotted lines represent the contributions of the background of pomeron plus (π, η) -exchange and the solid and dashed curves correspond to the full model predictions including a resonance of $3/2^+$ and $3/2^-$, respectively. In Figs. 5 and 6, the forward differential cross section as function

of energy where a bump is observed and the differential cross section as function of t are shown, respectively. The contribution of the resonance alone is also shown therein with dash-dotted and dash-dot-dotted lines corresponding to $3/2^+$ and $3/2^-$, respectively. We see that besides producing a bump in the forward differential cross section, the resonance improves the discrepancy between predictions of the background mechanisms and the data substantially in the t dependence of the differential cross

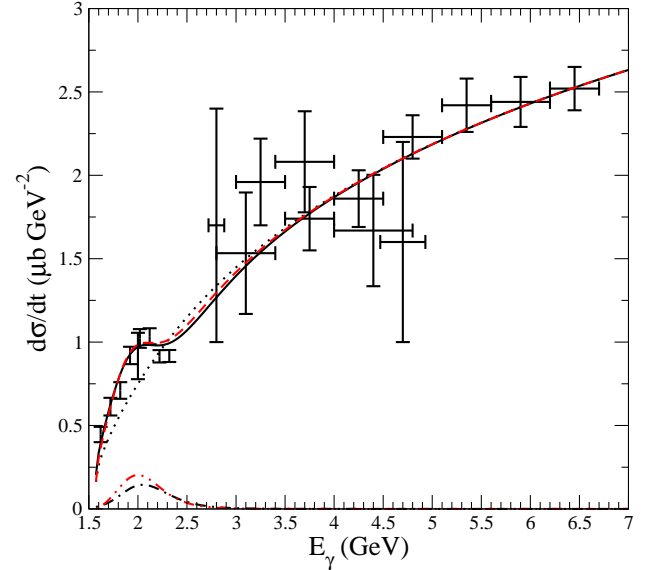


FIG. 5: The results obtained by employing a $J^P = 3/2^\pm$ resonances in our model for differential cross section of $\gamma p \rightarrow \phi p$ at forward direction as a function of the incoming photon energy E_γ , (b) differential cross section of $\gamma p \rightarrow \phi p$ as a function of $t + |t|_{\min}$ at eight different energies. Data is taken from Ref. [19]. The dotted lines are pomeron and t -channel contributions only. The full and dashed lines are the total contributions including $J^P = 3/2^+$ and $J^P = 3/2^-$ resonances, respectively. The dash-dotted and dash-dot-dotted lines are the resonant s - and u -channels contributions, respectively.

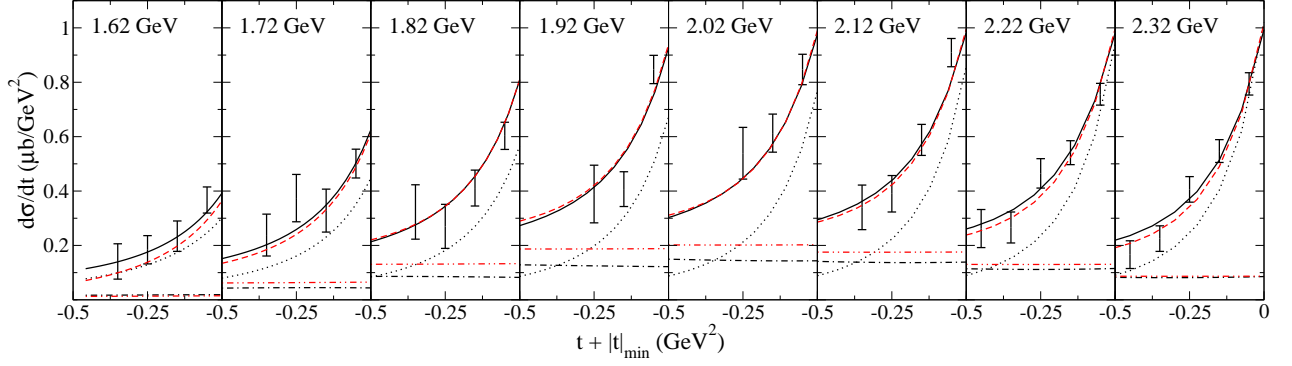


FIG. 6: The results obtained by employing a $J^P = 3/2^-$ resonance in our model for differential cross section of $\gamma p \rightarrow \phi p$ as a function of $t + |t|_{\min}$ at eight different energies. Data is taken from Ref. [19]. Notation is as in Fig. 5.

sections.

In Figs. 7-9, our model predictions for the SDME's in the three energy regions of $1.77 < E_\gamma < 1.97$, $1.97 < E_\gamma < 2.17$, and $2.17 < E_\gamma < 2.37$ GeV are shown together with the data of [16]. It is seen that in some cases, e.g., $\rho_{10}^0, \rho_{10}^1, \rho_{10}^2$ in $1.97 < E_\gamma < 2.17$, the nonresonant contribution alone already describes well the data and the resonance contributions are small. However, there are several cases that a $3/2^-$ resonance is indeed quite helpful to bridge the difference between background contribution and the data, especially for ρ_{00}^0 in all energy regions, though its corrections are in the wrong direction for $\rho_{1,-1}^1$ and $\rho_{1,-1}^2$ in the region of $1.77 < E_\gamma < 1.97$. The effect of a $3/2^+$ resonance is in general less conspicuous than that of a $3/2^-$ resonance.

The decay angular distributions $W(\cos \Theta)$, $W(\Phi - \Psi)$, $W(\Phi)$, $W(\Phi + \Psi)$, and $W(\Psi)$ in Gottfried-Jackson frame depend on six SDMEs via the following relations,

$$\begin{aligned}
 W(\cos \Theta) &= \frac{3}{2} \left[\frac{1}{2} (1 - \rho_{00}^0) \sin^2 \Theta + \rho_{00}^0 \cos^2 \Theta \right], \\
 W(\Phi) &= \frac{1}{2\pi} (1 - 2\text{Re}\rho_{1-1}^0 \cos 2\Phi), \\
 W(\Phi - \Psi) &= \frac{1}{2\pi} \{1 + 2P_\gamma(\rho_{1-1}^1 - \text{Im}\rho_{1-1}^2) \\
 &\quad \times \cos[2(\Phi - \Psi)]\}, \\
 W(\Phi + \Psi) &= \frac{1}{2\pi} \{1 + 2P_\gamma(\rho_{1-1}^1 + \text{Im}\rho_{1-1}^2) \\
 &\quad \times \cos[2(\Phi + \Psi)]\}, \\
 W(\Psi) &= \frac{1}{2\pi} [1 - P_\gamma(2\rho_{11}^1 + \rho_{00}^1) \cos 2\Psi], \quad (17)
 \end{aligned}$$

where the angles Θ , Φ , and Ψ are illustrated in Fig. 4. Here, they are measured at two different energy bins $1.97 - 2.17$ GeV and $2.17 - 2.37$ GeV within the range of $|t - t_{\max}| \leq 0.2$ GeV². In our work, they are calculated at the midpoint of each energy bin E_γ by weighing them

with the differential cross section as a function of t

$$W(E_\gamma, \Theta, \Phi, \Psi) = \frac{\int_{t_{\max}-0.2}^{t_{\max}} dt [d\sigma(E_\gamma, t)/dt] W(E_\gamma, t, \Theta, \Phi, \Psi)}{\int_{t_{\max}-0.2}^{t_{\max}} dt [d\sigma(E_\gamma, t)/dt]} \quad (18)$$

It is seen that the effect of the resonance, be it $3/2^+$ or $3/2^-$, is insignificant in most cases.

Based on the similarities in their masses and spin-parities, one might wonder whether the $3/2^-$ resonance found here can be identified as the $D_{13}(2080)$ as listed in PDG [11]. The coupling constants given Table I can be used to calculate the ratio of the helicity amplitudes

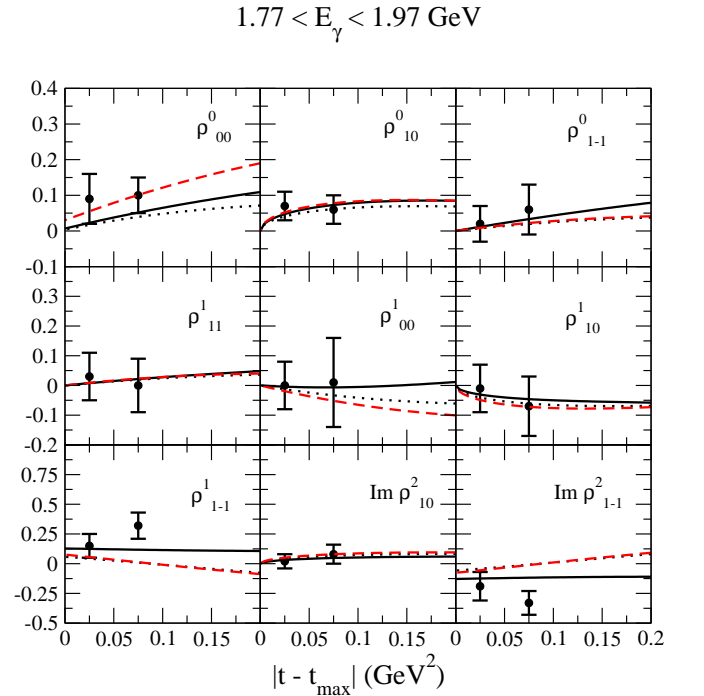


FIG. 7: Spin-density matrix elements in Gottfried-Jackson system as a function of t at $1.77 < E_\gamma < 1.97$ GeV. Notation is as in Fig. 5.

$A_{1/2}$ and $A_{3/2}$. However, we cannot determine their magnitudes since we have only the products of the coupling constants γNN^* and ϕNN^* . We obtain a value of $A_{1/2}/A_{3/2} = 1.05$, while it is -1.18 for $D_{13}(2080)$. Although their magnitudes are quite similar, they differ by a sign and we conclude that the resonance postulated here, if exists, cannot be identified with $D_{13}(2080)$.

B. Analysis on the composition of the bump structure

Our results for the forward differential cross sections of the $J^P = 3/2^\pm$ in Fig. 5 indicate constructive and destructive interferences of nonresonant and resonant amplitudes below and above the peak, respectively. Since the nonresonant amplitude is dominated overwhelmingly by Pomeron amplitude, which is almost completely imaginary, it seems to imply that the sign-changing component of the resonant part must then be also imaginary. However, it is well-known that the imaginary part of resonance amplitude is sign definite while the sign-changing component of a resonant amplitude is real.

In order to understand this, let us decompose the forward differential cross section ($\propto |T|^2$) into its nonresonant, resonant, and interference terms

$$|T|^2 = |T_{NR}|^2 + |T_R|^2 + 2\text{Re}(T_{NR}T_R^*) \quad (19)$$

$$1.97 < E_\gamma < 2.17 \text{ GeV}$$

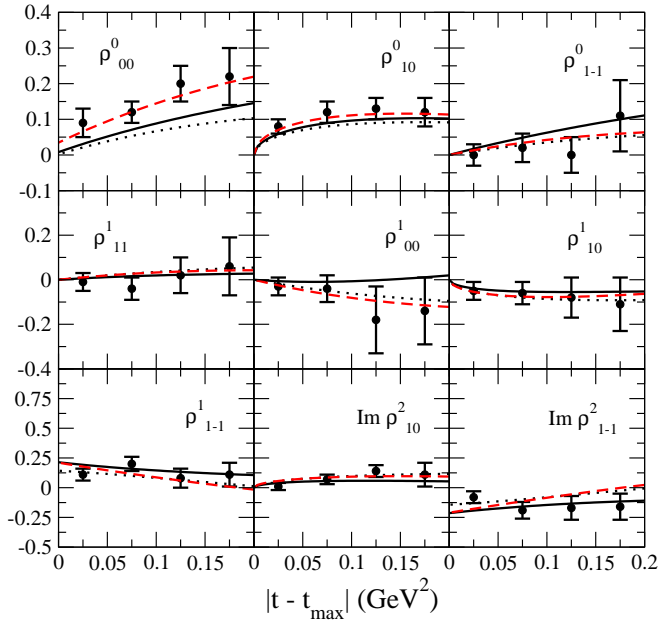


FIG. 8: Spin-density matrix elements in Gottfried-Jackson system as a function of t at $1.97 < E_\gamma < 2.17$ GeV. Notation is as in Fig. 5.

$$2.17 < E_\gamma < 2.37 \text{ GeV}$$

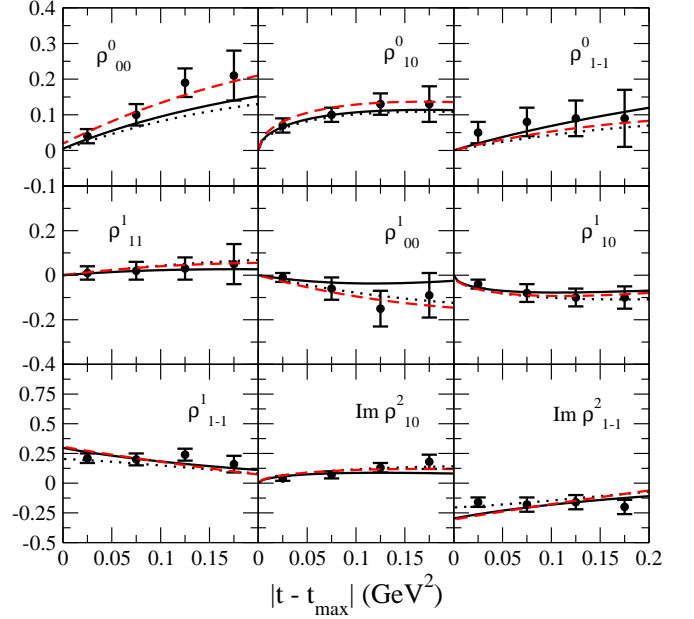


FIG. 9: Spin-density matrix elements in Gottfried-Jackson system as a function of t at $2.17 < E_\gamma < 2.37$ GeV. Notation is as in Fig. 5.

in which T , T_{NR} , and T_R are the total, nonresonant, and resonant amplitudes, respectively. We also have

$$T_{NR} = T_P + T_M \quad (20)$$

where T_P and T_M are the Pomeron and meson-exchange amplitude, respectively.

However, the decompositions of $2\text{Re}(T_{NR}T_R^*)$, which are given in the Fig. 11 for both $J^P = 3/2^\pm$ resonances show that while the interference between pomeron and the resonant amplitudes are sign definite, the interference between the meson-exchange and resonant amplitudes are sign changing. The key here is that the interference between meson-exchange and resonant amplitudes is sign changing as well as comparable in size to that of the pomeron and resonant amplitudes. Therefore the meson-exchange mechanisms are indeed crucial in producing the peaking behavior observed in ϕ -photoproduction reaction.

C. Effects on ωN channel

We can further study if introducing the postulated resonance would improve the theoretical description of the ωN channel. The conventional "minimal" parametrization relating ϕNN^* and ωNN^* is

$$g_{\phi NN^*} = -\tan \Delta\theta_V x_{\text{OZI}} g_{\omega NN^*}, \quad (21)$$

with $\Delta\theta_V \simeq 3.7^\circ$ corresponds to the deviation from the ideal $\phi - \omega$ mixing angle. Here, x_{OZI} is called the OZI-

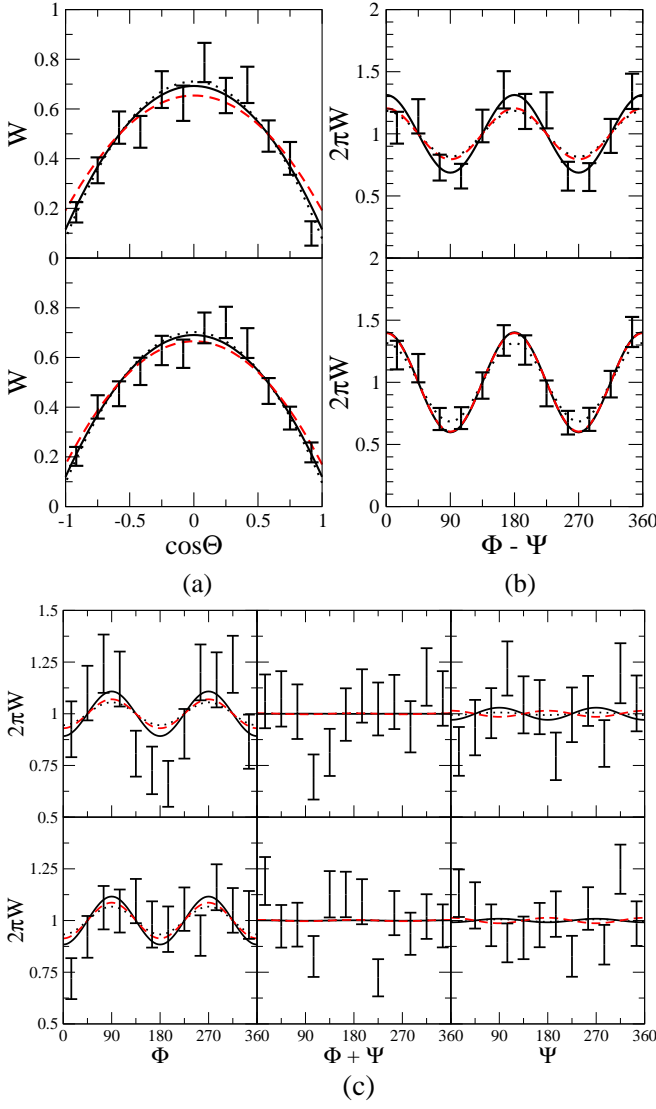


FIG. 10: Decay angular distributions (a) $W(\cos \Theta)$, (b) $W(\Phi - \Psi)$, (c) $W(\Phi)$, $W(\Phi + \Psi)$, and $W(\Psi)$, at photon LAB energies 1.97 – 2.17 GeV (upper panels) and 2.17 – 2.37 GeV (lower panels) within the range of $|t - t_{\max}| \leq 0.2 \text{ GeV}^2$. Notation is as in Fig. 5.

evading parameter and the larger value of x_{OZI} would indicate larger strangeness content of the resonance.

Here, we estimate the amplitudes of ω photoproduction without the postulated resonance by employing the study of Ref. [23] which employs the nucleon resonances predicted by Refs. [25, 26]. In Fig. 12, it is seen that the prediction of their model for the t -dependence of differential cross section at $W = 2.105 \text{ GeV}$, given in dotted line, still exhibits substantial discrepancy with the most recent experimental data [27] for $|t| > 0.75 \text{ GeV}^2$. By adding resonance postulated here to the model of Ref. [23] with $x_{\text{OZI}} = 12(9)$ for $J^P = 3/2^-$ ($J^P = 3/2^+$) whose predictions are given by the solid black (dashed red) line in Fig. 12, we see that the differential cross section at $W = 2.105$ and 2.305 GeV can be reproduced

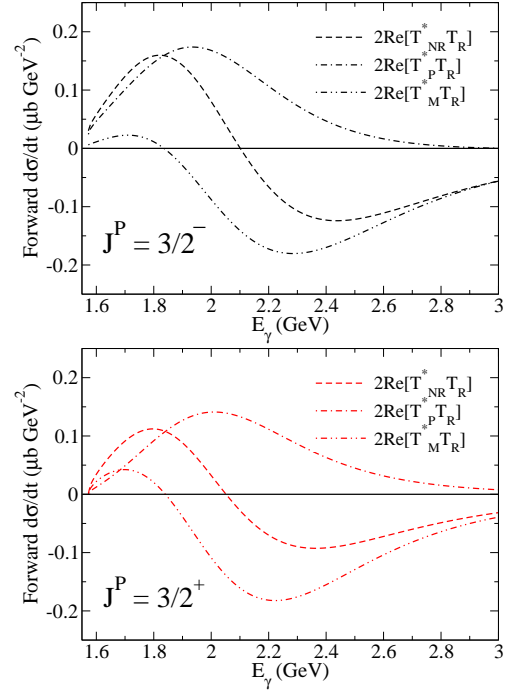


FIG. 11: Detailed analysis of the differential cross section at forward angle shows the composition of the observable.

with roughly the correct strength. The other energies do not show as much improvement due to the fact that they are far from the energy of the resonance. The large values of x_{OZI} would imply that the resonances we propose here contains considerable amount of strangeness contents. It is interesting to note that $J^P = 3/2^+$ resonance requires a smaller value for x_{OZI} compared to $J^P = 3/2^-$ resonance. This means that a $J^P = 3/2^+$ resonance requires less strangeness content in order to explain the experimental data.

D. Strangeness content of the resonance

The resonance proposed here appears to have a large OZI evasion parameter x_{OZI} which would lead one to ask whether this is reasonable. In this section, we will estimate the strangeness content of the resonance. We can write, for the wavefunction of the resonance

$$|N^*\rangle = x|uud\rangle + z_u|uudu\bar{u}\rangle + z_d|uudd\bar{d}\rangle + z_s|uuds\bar{s}\rangle \quad (22)$$

where x is real but z_u , z_d , and z_s are all complex and $|x|^2 + |z_u|^2 + |z_d|^2 + |z_s|^2 = 1$. Let us define

$$Z \equiv \frac{\mathcal{M}(N^* \rightarrow \phi_{id}N)}{\mathcal{M}(N^* \rightarrow \omega_{id}N)} \quad (23)$$

where $\mathcal{M}(N^* \rightarrow V_{id}N)$ is the amplitude of the decay of N^* to $V_{id}N$ where the subscript id denotes that the vector meson V is in its ideal state. For example, ϕ_{id} consists of pure $s\bar{s}$ with no $u\bar{u}$ or $d\bar{d}$ mixture.

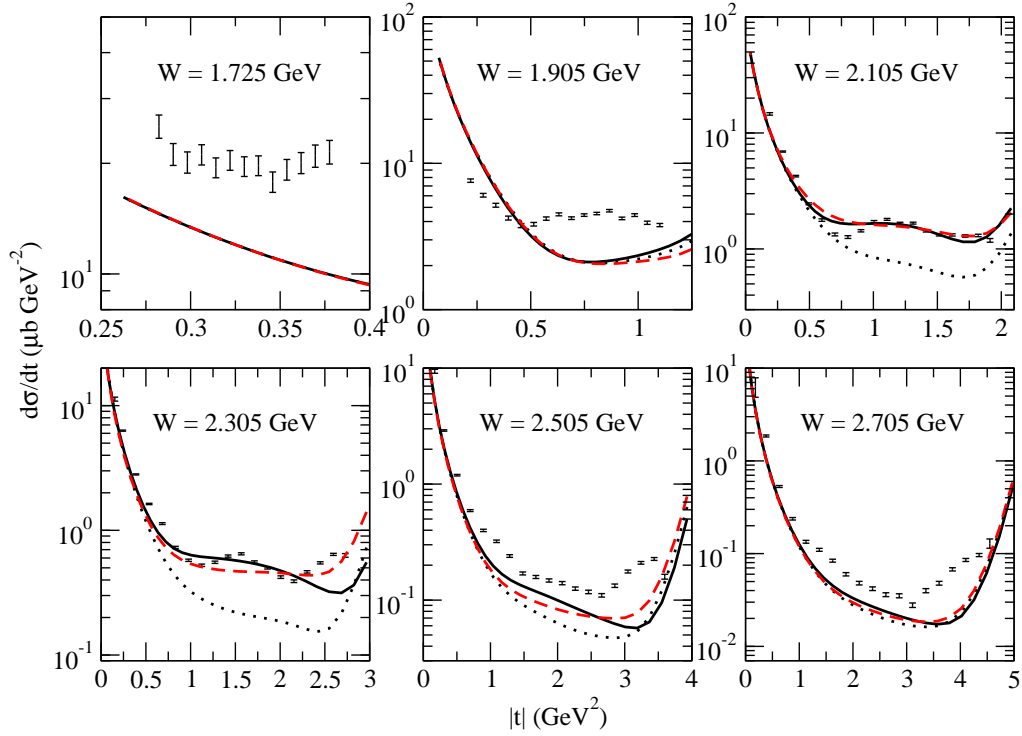


FIG. 12: Predictions of the effects of the postulated resonances to the differential cross section of ω photoproduction at CM energies $W = 1.725, 1.905, 2.105, 2.305, 2.505$, and 2.705 GeV. Notation is as in Fig. 5.

We can obtain Z experimentally from

$$Z = \frac{Z_{\text{phys}} + \tan \Delta\theta_V}{1 - Z_{\text{phys}} \tan \Delta\theta_V} \quad (24)$$

where

$$Z_{\text{phys}} \equiv \frac{\mathcal{M}(N^* \rightarrow \phi N)}{\mathcal{M}(N^* \rightarrow \omega N)} \quad (25)$$

is defined for the physical particles ϕ and ω . Here, Z_{phys} can be estimated from $g_{\phi NN^*}/g_{\omega NN^*} = -x_{\text{OZI}} \tan \Delta\theta_V$. Notice that $Z = 0$ when $x_{\text{OZI}} = 1$ which is the case of the ordinary OZI violation without strangeness content.

Now, let us calculate Z theoretically from constituent quark model by introducing \mathcal{M}_3 and \mathcal{M}_5 which are de-

picted in Fig. 13(a) and (b). We can write then

$$\mathcal{M}(N^* \rightarrow \phi_{id} N) = z_s \mathcal{M}_5$$

$$\mathcal{M}(N^* \rightarrow \omega_{id} N) = x \mathcal{M}_3 + \frac{1}{\sqrt{2}} (z_u + z_d) \mathcal{M}_5. \quad (26)$$

Let us now introduce $z_q \equiv \delta_q a_q$ where $q = u, d, s$ which separate the phases δ_q and the magnitudes a_q of the amplitudes. Further, let's introduce $c_u \equiv a_s/a_u$ and $c_d \equiv a_d/a_s$. After substituting, we have

$$Z = \frac{\delta_s a_s \mathcal{M}_5}{x \mathcal{M}_3 + \frac{1}{\sqrt{2}} (\delta_u c_u + \delta_d c_d) a_s \mathcal{M}_5} \quad (27)$$

which can be finally solved for a_s^2 to give the probability of the strangeness content

$$P_s \equiv a_s^2 = \frac{1}{1 + c_u^2 + c_d^2 + \left(\frac{D}{N}\right)^2 F^{-2}} \quad (28)$$

where

$$\begin{aligned} N &\equiv Z \\ D &\equiv 1 - \frac{1}{\sqrt{2}} Z (\delta_u \delta_s^* c_u + \delta_d \delta_s^* c_d). \end{aligned} \quad (29)$$

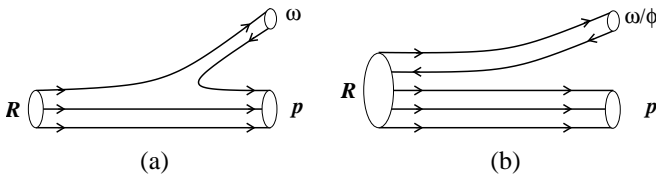


FIG. 13: Quark-flow diagrams of the processes that give rise to the amplitudes (a) \mathcal{M}_3 and (b) \mathcal{M}_5 .

There is a requirement that $\left(\frac{D}{N}\right) F^{-1}$ must be real and positive. Since the variables D , N , and F depend on

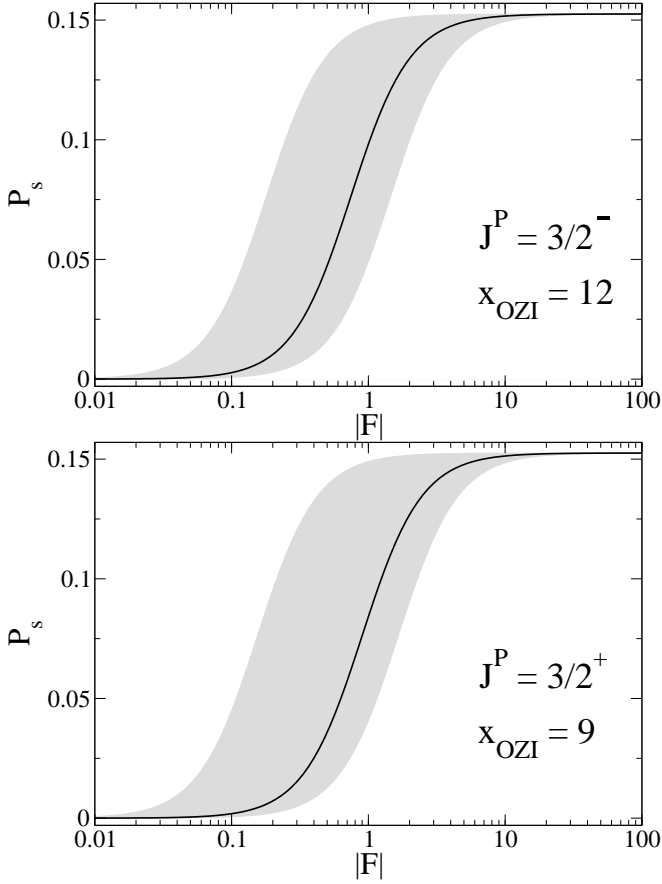


FIG. 14: Strangeness content of the resonances P_s for $x_{\text{OZI}} = 12$ and $x_{\text{OZI}} = 9$ corresponding to $J^P = 3/2^-$ and $J^P = 3/2^+$, respectively, as functions of $|F|$. The shaded areas show the 95% probability range after the phases are randomly varied. The solid black lines are the median.

δ_u , δ_d , δ_s , as well as the phases of Z , \mathcal{M}_3 and \mathcal{M}_5 , one can ask whether such a combination can possibly be found. However, the phases of \mathcal{M}_3 and \mathcal{M}_5 can always be adjusted to satisfy the requirement. Of course in reality, all these phases are fixed. However, due to our limited knowledge about solving the underlying QCD dynamics, we treat all of them as adjustable parameters. For the values of c_u and c_d , we assume that $P_{u,d}/P_s = (m_s/m_{u,d})^2$ according to Ref. [29]. Therefore, $c_u = c_d = m_s/m_{u,d}$ where $m_s = 0.5$ GeV and $m_{u,d} = 0.3$ GeV are the constituent quark masses for the strange and up/down quarks.

Since the ratio of the strength $|F|$ between \mathcal{M}_3 and \mathcal{M}_5 is not known, we vary the value of $|F|$ from 0.01 to 100, which correspond to $|\mathcal{M}_5| = 100|\mathcal{M}_3|$ and $|\mathcal{M}_3| = 100|\mathcal{M}_5|$, respectively. The range of P_s within 95% probability obtained by randomly varying the phases are given by the shaded area in Fig. 14 while the median value are given by the solid black lines. Notice that the lower bound of P_s is determined by $D_{\text{max}} = 1 + \frac{1}{\sqrt{2}}|Z|(c_u + c_d)$ while the upper bound is by $D_{\text{min}} = 0$. The upper bound has the value of $P_s = 15.2\%$, which

corresponds to a resonance with 100% five-quark content after including the contributions from $uudu\bar{u}$ and $uudd\bar{d}$.

A rather broad range of P_s also reflects the situation faced in the efforts of determining the strangeness content in the proton, which is stable and can be more directly studied. Recent studies give estimates ranging from $0.025 - 0.058\%$ [30] to $2.4 - 2.9\%$ [31].

E. Polarization observables

Since the fit results from both resonances are rather similar, we need to find key observables that can help us to distinguish them. Here, we show some predictions on the polarization observables predicted at photon laboratory energy $E_\gamma = 2.0$ GeV near the resonance position. Three single polarization observables: asymmetries of the polarized beam Σ_x , polarized target T_y , and recoil polarization $P_{y'}$ are given in Fig. 15 while four double polarization observables: beam-target (BT) asymmetries C_{yx}^{BT} , C_{yz}^{BT} , C_{zx}^{BT} , and C_{zz}^{BT} , with the photon beam and the nucleon target polarized, are given in Fig. 16. The notation of the polarization observables follows Ref. 15.

It can be concluded from Figs. 15 and 16 that while all the observables presented are reasonably distinct enough to distinguish the parities of the $J = 3/2$ resonances, the single polarization observable Σ_x is actually the most distinct based on the opposite sign of the curves produced by the two parities. Therefore, we would recommend the use of Σ_x to resolve the ambiguity surrounding the parity of the resonance.

IV. SUMMARY AND CONCLUSIONS

In summary, we present the details and more extensive results of the analysis of the near-threshold bump structure in the forward differential cross section of the ϕ -meson photoproduction to determine whether it is a signature of a resonance. The analysis is carried out in an effective Lagrangian approach which includes Pomeron and (π, η) exchanges in the t channel and contributions from the s - and u -channel excitation of a postulated resonance.

Besides the differential cross sections at forward angle as function of photon energy and as function of t , the recent data on nine spin-density matrix elements at three photon energies reported by the LEPS collaboration are used, instead of the decay angular distributions of the ϕ meson as was done before [14], which depend only on six spin-density matrix elements as was done before, to constrain the model. Moreover, the new spin-density matrix element data are given as a function of t , while the previous decay angular distribution data are not. Therefore, the new set of data are expected to give more strict constraints on the resulting resonance parameters.

We confirm that indeed the bump structure can only be explained with an assumption of the excitation of a

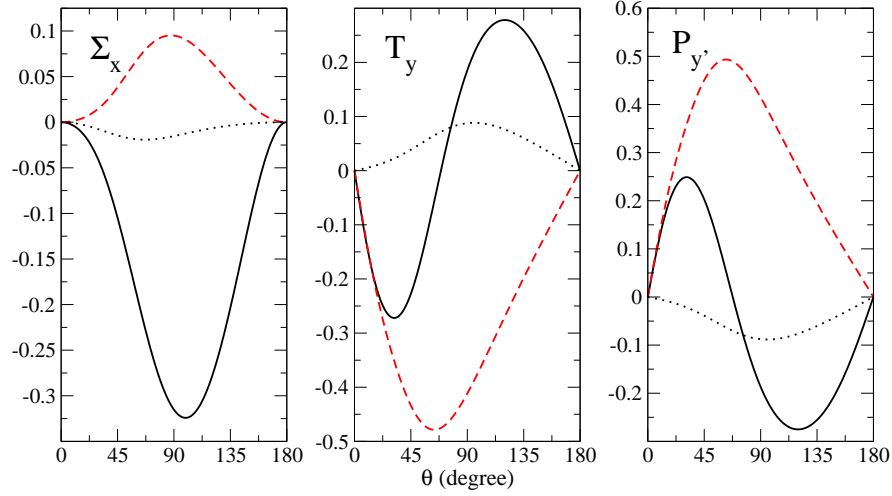


FIG. 15: Single polarization observables: polarized beam Σ_x , polarized target T_y , and recoil polarization $P_{y'}$ asymmetries, taken at photon laboratory energy $E_\gamma = 2.0$ GeV. The dotted lines denote the t -channel contributions, while the solid black and red lines are contributions from $J^P = 3/2^-$ and $J^P = 3/2^+$, respectively.

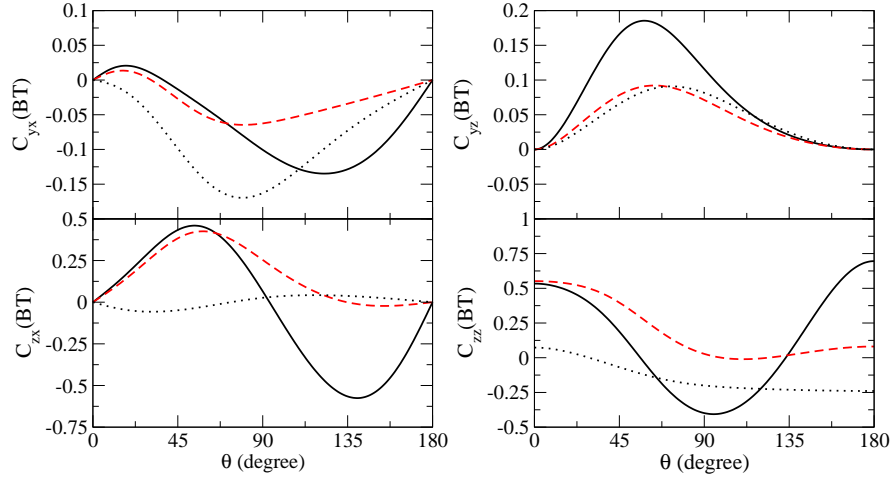


FIG. 16: Double polarization observables: beam-target (BT) asymmetries C_{yx}^{BT} , C_{yz}^{BT} , C_{zx}^{BT} , and C_{zz}^{BT} , with photon beam and nucleon target polarized, taken at photon laboratory energy $E_\gamma = 2.0$ GeV. Notation is as in Fig.15.

resonance of spin $3/2$. We conclude that indeed the bump structure as reported by LEPS, can only be explained with an assumption of the excitation of a resonance of spin $3/2$, as previously reported. However, both parities of (\pm) can account for the data equally well with almost identical mass of 2.08 ± 0.04 GeV and width of 0.501 ± 0.117 and 0.570 ± 0.159 for $3/2^-$ and $3/2^+$, respectively.

The helicity amplitudes of the $J^P = 3/2^-$ resonance calculated from the obtained coupling constants gives a ratio of $A_{1/2}/A_{3/2} = 1.05$ which differs in sign from the value of -1.18 of $D_{13}(2080)$ given by the PDG. Therefore, we conclude that the $J^P = 3/2^-$ resonance cannot be identified as $D_{13}(2080)$. The ratio of helicity amplitudes of the $J^P = 3/2^+$ resonance is obtained to be of $A_{1/2}/A_{3/2} = 0.89$.

Some of the single and double polarization observables which are sensitive to the parity of the resonance, includ-

ing beam asymmetry Σ_x , target asymmetry T_x , recoil asymmetry P_x , and beam-target asymmetry $C_{ij}(BT)$, near the resonance peak are also given. Measurement of these quantities would be most helpful in further substantiating whether the nonmonotonic behavior is indeed a signature of resonance as well as resolving its parity. Of all the observables, we find that the single polarization observable of beam asymmetry Σ_x provides the best way to resolve the parity of the resonance since they are of opposite signs with different parity.

We have also investigated the effects of the postulated resonances to the differential cross section of ω photo-production as a function of t within the model of [23]. We find that the proposed resonance improves the agreement with the data, especially around the photon LAB energy of 2.1 GeV, if large values of OZI-evading parameter $x_{\text{OZI}} = 12$ and $x_{\text{OZI}} = 9$ for $J^P = 3/2^-$ and

$J^P = 3/2^+$ resonances, respectively, are assumed. Here, again, both resonances are equally capable of improving the discrepancy between the data and the predictions of [23]. It adds support for the resonance we postulate. We argue that the large values of OZI-evading parameter x_{OZI} found imply that the postulated resonance might contain a strangeness content of $P_s = 0.1 \sim 15\%$. If the postulated resonance contains considerable amount of strangeness, then it could couple strongly to, say, $K\Lambda$ channel. Question would then arise on how the coupled-channel effects would modify the low-energy behavior of the nonresonant amplitude employed in this investigation. This can be answered only with a full coupled-channel calculations as was done in [15].

Acknowledgments

We would like to thank Drs. W.C. Chang, Atsushi Hosaka, A.I. Titov, T.-S.H. Lee, Yongseok Oh, and Sho Ozaki for useful discussions and/or correspondences. This work was supported in parts by National Science Council of the Republic of China (Taiwan) under grant NSC99-2112-M002-011. We would also like to acknowledge the help from National Taiwan University High-Performance Computing Center in providing us with a fast and dependable computation environment which is essential in completing this work.

-
- [1] T. H. Bauer, R. D. Spital, D. R. Yennie and F. M. Pipkin, *Rev. Mod. Phys.* **50**, 261 (1978).
 - [2] A. Donnachie and P. V. Landshoff, *Phys. Lett. B* **185**, 403 (1987); *Nucl. Phys. B* **244**, 322 (1984); *Nucl. Phys. B* **267**, 690 (1986); *Nucl. Phys. B* **311**, 509 (1989).
 - [3] R. A. Williams, *Phys. Rev. C* **57**, 223 (1998).
 - [4] Y. S. Oh and H. C. Bhang, *Phys. Rev. C* **64**, 055207 (2001).
 - [5] Q. Zhao, J.-P. Didelez, M. Guidal and B. Saghai, *Nucl. Phys. A* **660**, 323 (1999); Q. Zhao, B. Saghai and J. S. Al-Khalili, *Phys. Lett. B* **509**, 231 (2001).
 - [6] A. I. Titov, T.-S. H. Lee, *Phys. Rev. C* **67**, 065205 (2003).
 - [7] A. I. Titov, T.-S. H. Lee, H. Toki, and O. Streltsova, *Phys. Rev. C* **60**, 035205 (1999).
 - [8] A. I. Titov, Y. S. Oh and S. N. Yang, *Phys. Rev. Lett.* **79**, 1634 (1997); A. I. Titov, Y. Oh, S. N. Yang, and T. Morii, *Nucl. Phys. A* **684**, 354 (2001).
 - [9] A. I. Titov, Y. Oh, S. N. Yang, and T. Morii, *Phys. Rev. C* **58**, 2429 (1998).
 - [10] T. Mibe *et al.* (LEPS Collaboration), *Phys. Rev. Lett.* **95**, 182201 (2005) and references therein.
 - [11] K. Nakamura *et al.* (Particle Data Group), *J. Phys. G* **37**, 075021 (2010).
 - [12] H. J. Besch *et al.*, *Nucl. Phys. B* **70**, 257 (1974).
 - [13] CLAS Collaboration, E. Anciant *et al.*, *Phys. Rev. Lett.* **85**, 4682 (2000).
 - [14] A. Kiswandhi, J.J. Xie, and S.N. Yang, *Phys. Lett. B* **691**, 214 (2010).
 - [15] S. Ozaki, A. Hosaka, H. Nagahiro, and O. Scholten, *Phys. Rev. C* **80**, 035201 (2009); **81**, 059901(E) (2010).
 - [16] W. C. Chang *et al.* (LEPS Collaboration), *Phys. Rev. C* **82**, 015205 (2010).
 - [17] A. I. Titov and B. Kämpfer, *Phys. Rev. C* **76**, 035202 (2007).
 - [18] C.-T. Hung, S.N. Yang, and T.-S. Lee, *Phys. Rev. C* **64**, 034309 (2001).
 - [19] Durham High Energy Physics database (HEPDAT) (<http://www.slac.stanford.edu/spires/hepdata>).
 - [20] W.-T. Chiang, S. N. Yang, M. Vanderhaeghen, and D. Drechsel, *Nucl. Phys. A* **723**, 205 (2003).
 - [21] V. Pascalutsa, M. Vanderhaeghen, and S. N. Yang, *Phys. Rept.* **437**, 125 (2007).
 - [22] T. Feuster and U. Mosel, *Nucl. Phys. A* **612**, 375 (1997).
 - [23] Y. Oh, A. I. Titov, and T.-S.H. Lee, *Phys. Rev. C* **63**, 025201 (2001).
 - [24] K. Schilling, K. Seyboth, and G. Wolf, *Nucl. Phys. B* **15**, 397 (1970).
 - [25] S. Capstick and W. Roberts, *Phys. Rev. D* **49** No. 9 (1994).
 - [26] S. Capstick, *Phys. Rev. D* **46** No. 7 (1992).
 - [27] M. Williams *et al.*, *Phys. Rev. C* **80**, 065208 (2009).
 - [28] J. Ellis, M. Karliner, D.E. Kharzeev, M.G. Sapozhnikov, *Phys. Lett. B* **353**, 319 (1995); G. Höhler *et al.*, *Nucl. Phys. B* **114**, 505 (1976); S. Dubnicka, *Nuovo Cimento A* **100**, 1 (1988).
 - [29] S.J. Brodsky, P. Hoyer, C. Peterson, and N. Sakai, *Phys. Lett. B* **93**, 451 (1980); S.J. Brodsky, C. Peterson, and N. Sakai, *Phys. Rev. D* **23**, 2745 (1981).
 - [30] A. Kiswandhi, H.-C. Lee, and S.N. Yang, *Phys. Lett. B* **704**, 373 (2011).
 - [31] W.C. Chang and J.C. Peng, *Phys. Lett. B* **704**, 197 (2011), *Phys. Rev. Lett* **106**, 252002 (2011).